Classification of Image Edges

Hanna Chidiac et Djemel Ziou
Département de Mathématiques et d'Informatique,
Faculté des Sciences,
Université de Sherbrooke,
Sherbrooke (Qc), Canada, J1K 2R1
{chidiac, ziou}@dmi.usherb.ca

Abstract

Edges are relevant information for image representation. In this paper, we propose an algorithm for the classification of *step*, *concave slope*, *convex slope*, *roof*, *valley* and *staircase* edges. The importance of the classification is that it simplifies several problems in artificial vision and image processing, by associating specific processing rules to each type of edge. Our classification is based on the behavioral study of these edges with respect to differentiation operators and scale. The first directional derivative, the gradient and the Laplacian are used as operators. We test our algorithm on synthetic and real grey-level images. In most cases, the classification obtained corresponds to the intensity profile of the image.

1 Introduction

Edges are the most common features in an image; they are local variations in the image function. We limit ourselves here to the study of *step*, *concave slope*, *convex slope*, *roof*, *valley* and *staircase* edge types. These models cover the majority of edge types which can be generated by physical contours of a scene. The majority of existing edge detectors are intended for only one edge type. This is a significant limitation, because the consideration of several edge types will simplify a number of problems in artificial vision and image processing. Thus it is necessary to identify the edge types present in an image, whether by using several detectors or only one. In this paper, we are interested in using only one detector, so edge classification is required. The classification of edges consists in associating, with characteristic points of the image, the type of intensity variation which takes place at each point. In the literature, there is little work on classification. We present an algorithm based on the simultaneous use of inflection points of the first directional derivative or characteristic points of the gradient image, and those of the Laplacian image. The classification rules are derived from edge behavior with respect to differentiation operators and scale.

In Section 2, we summarize existing research on the detection and classification of edges. In Section 3, we present the edge models mentioned above. Then, we study their behavior when differentiation operators are applied. In Section 4, we study this behavior in the scale space. In Section 5, we present the classification algorithm. To illustrate the classification rules, we consider the case of *step*. In Section 6, we test our detector on synthetic and real images. Finally, a short discussion is presented in Section 7.

2 Related Work

Parallel to the continual development of edge detection algorithms, methods are necessary for their evaluation [9], and an overview of research in edge detection is needed [25]. In this section we cite those existing edge detectors which are most commonly used and are regarded as optimal. Detectors of *step* edges are the ones usually mentioned in the literature. In general, these edges correspond to discontinuities in the image function, and these discontinuities are generated by the borders of objects in the scene. The majority of *step* detectors involves two operations: filtering and differentiation. Lowpass filters are the most often used [2, 5, 18], while the most common operators are the gradient [2, 5], the Laplacian [13, 10], and the second directional derivative [8]. *Step* edges are localized as maxima of the gradient modulus taken in the direction of the gradient, or as zero-crossings of the Laplacian or the second derivative along the gradient direction.

Contrary to *step* detectors, those for other type of edges are rather rare, because their usefulness was understood later. Consideration of these types is unavoidable for several reasons: for instance, some approaches to the acquisition of 3D information require the determination of all types of edges (e.g., *"shape from contour"* [13, 16]). Furthermore, the images of fingerprints, roads or characters contain thin lines difficult to locate by a *step* detector. We present some of these detectors below. Haralick [7] detects lines at

zero-crossings of the first derivative taken in the direction maximizing the second directional derivative. Giraudon [6] identifies lines at the local extrema of the Laplacian image. Using Canny's criteria, Ziou [24] proposes an optimal line detector based on recursive filtering. Finally, Koundinya and Chanda [12] define a plausibility measurement for lines and they carry out a chaining using heuristic search algorithms. It should be noted that each of these detectors is generally intended for only one type of edge.

Though the classification of edges is a significant task in computer vision, it is rarely mentioned in the literature. In what follows, we underline some of the work done on classification which we have encountered in our search. Morrone, Venkatesh and Owens [14, 20] use a quadrature pair of filters to detect various types of edges. Robey, West and Venkatesh [17] propose a method to extract and classify occlusion/non-occlusion, shade and specularity edges on a simulated image. This method is based on ray tracing techniques. Zhang and Bergholm [23] classify *step, peak* and *asymmetrical peak* edges by using their behavior in the scale space. Catanzariti [3] classifies *step, slope* and *roof* edges. He convolved the image with a set of Gabor filters and then used a maximum-likelihood classification criterion to sort all pixels into a number of predefined edge categories. Finally, Beltran, Garcia-Lucia and Navarro [1] detect and classify *step, slope, staircase* and *pulse* (*peak*) edges using a neural network trained with the *discrete wavelet transform* coefficients for each edge profile.

3 Effects of Differentiation Operators on Edges

In this section we present some models of edges, and examine their behavior in the case of the gradient or the first directional derivative in the gradient direction[1], and in the case of the Laplacian. We limit our study to *step, concave slope, convex slope, roof, valley* and *staircase* edges (Figure 1). *Peaks* are implicitly considered in our work, since after smoothing, a *peak* will be similar to a *roof* or a *valley*. These models cover the majority of edges which can be generated by physical contours of the scene [4], hence their importance to represent an image.

We carry out this study in the discrete case, without noise, and considering a small scale of smoothing to avoid its effect on edges. For the sake of simplicity the edge profiles illustrated in Figures 1, 2, 3, 4 and 5 are plotted as continuous functions.

At the *step* edge (Figure 2), the module of the gradient has a maximum which we call $maximum_g$, and the Laplacian yields a zero-crossing which we call *zero-crossing*$_L$.

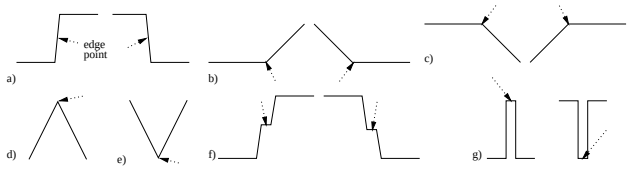

Figure 1: Models of ideal edges. The edge point in each model is indicated by an arrow. a) *Step*. b) *Concave slope*. c) *Convex slope*. d) *Roof*. e) *Valley*. f) *Staircase*. g) *Peak*.

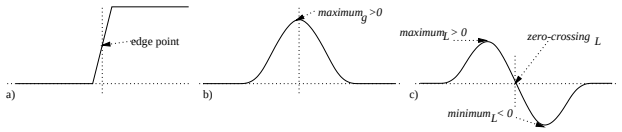

Figure 2: a) *Step* edge. b) The gradient image. c) The Laplacian image.

At *concave slope* and *convex slope* edges, the first directional derivative is a *step* whose inflection point locates the edge (Figure 3). In the case of *concave slopes* (resp. *convex slopes*) the Laplacian generates a positive maximum (resp. a negative minimum) which we call $maximum_L$ (resp. $minimum_L$).

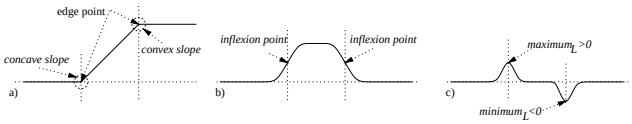

Figure 3: a) *Concave slope* and *convex slope* edges. b) The first directional derivative. c) The Laplacian image.

At symmetric *roof* and *valley* edges (Figure 4.a), the module of the gradient has a minimum equal to zero (Figure 4.b) which we call $zero_g$, and the Laplacian provides a negative minimum in the case of a *roof* and a positive maximum in the case of a *valley* (Figure 4.c). If *roof* and *valley* edges are asymmetrical (Figure 4.a'), the module of the gradient of each is a positive minimum (Figure 4.b') which we call $minimum_g$. The response of the Laplacian operator to these edges is similar to the symmetrical case (Figure 4.c').

At a *staircase* edge (Figure 5), the module of the gradient is often a positive minimum and the Laplacian yields a zero-crossing.

It is well known that at a *step* edge, the gradient direction is perpendicular to its tangent. Usually, the gradient modulus of a *concave slope, convex slope, roof, valley* and *staircase* is not zero. In fact, in realistic images the width of a *staircase* is not large and the *roofs/valleys* are not symmetric. Generally the gradient direction is perpendicular to the tangents of the *concave slope, convex slope* and *staircase* edges, and less often to the tangents of the *roof* and *valley* edges [4].

[1] It should be noted that in our implementation we do not distinguish between directions θ and $\theta + k\pi$. So the first directional derivative in the gradient direction is not equal to the gradient modulus; in fact we can have negative values.

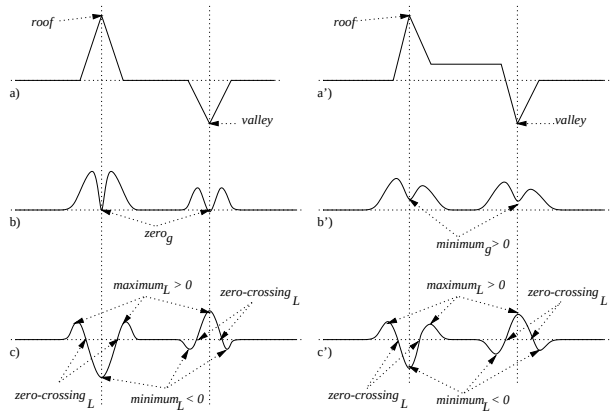

Figure 4: a) *Roof* and *valley*. a') Asymmetrical *roof* and *valley*. b), b') The gradient image. c), c') The Laplacian image.

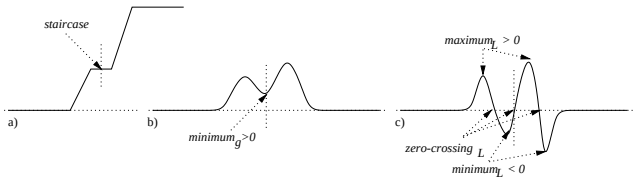

Figure 5: a) *Staircase* edge. b) The gradient image. c) The Laplacian image.

4 Effect of Scale on Edges

The numerical differentiation of an image is an ill-posed problem. To make the differentiation robust, one uses the technique of regularization which consists in imposing new criteria on the problem of differentiation, to restrict the solution space. This can be carried out by smoothing the image with a particular filter [19] having a form similar to the Gaussian function [15]. Differentiation can be achieved by convolution of the image with derivatives of this filter. A filter or its derivatives can be represented by a function $f(x, y, a)$, where a is the scale of the filter or a regularization parameter. For example, the scale of the Gaussian is the standard deviation. Generally, the smoothing operation blurs the edges and abrupt variations in the image grey levels. The blurring depends on the value of the scale. If the scale is large, obvious or unsharp edges are picked up; whereas if the scale is small, fine details are obtained. In consequence, the smoothing operation regulates robustess to noise; however, it can modify the structure of the image in an undesirable way: for instance, by elimination and displacement of edges, creation of new edges or modification of the types of some edges. These effects are accentuated when the scale increases. In what follows, we study the effect of the scale on edges. We will consider the case of the Gaussian filter defined by $g_\sigma(x) = \frac{1}{\sqrt{2\pi}\,\sigma} e^{\frac{-x^2}{2\sigma^2}}$, where σ is the scale. To simplify our analysis, we limit ourself to the 1D case. The main results in 1D remain valid in 2D. We do not consider the noise problem in our study of edge behavior in the scale space; in fact, experimentation has shown that the effect of scale on the edges presented in this section is not affected by the presence of noise.

An ideal *step* is defined by $m_i(x) = cu(x)$, where $c > 0$ represents the contrast and u is Heaviside's function, defined by

$$u(x) = \begin{cases} 1 & \text{if } x \geq 0 \\ 0 & \text{otherwise} \end{cases}$$

The first, second and third derivatives of the smoothed *step* are: $m'(x) = c(u * g_\sigma)'(x) = c(u' * g_\sigma)(x) = cg_\sigma(x)$, $m''(x) = \frac{-cx}{\sigma^2} g_\sigma(x)$, $m'''(x) = \frac{c}{\sigma^2}(\frac{x^2}{\sigma^2} - 1) g_\sigma(x)$. For all σ, $m'(x)$ has a positive maximum at $x = 0$; $m''(x)$ is equal to zero at this point, with a positive maximum at $x = -\sigma$ and a negative minimum at $x = \sigma$ (Table 1). As σ increases, $m'(0) = \frac{c}{\sqrt{2\pi}\sigma}$ decreases, and the maximum and minimum of $m''(x)$ move away from each other.

x	- ∞	- σ		0		σ	+ ∞
m'(x)	+		+	*max*	+		+
m''(x)	+	*max*	+	0	-	*min*	-
m'''(x)	+	0	-	-	-	0	+

Table 1: Effect of σ on a *step* edge.

Let us study the effect of scale on the *concave slope* edge. The case of the *convex slope* is similar. An ideal *concave slope* is defined by

$$r_i(x) = \begin{cases} 0 & \text{if } x < 0 \\ ax & \text{otherwise (where } a > 0). \end{cases}$$

The convolution of $r_i(x)$ with the Gaussian filter g_σ is $r(x) = ax\phi(x) + a\sigma^2 g_\sigma(x)$, where $\phi(x) = \int_{-\infty}^{x} g_\sigma(t)dt$. The first, second and third derivatives of $r(x)$ are $r'(x) = a\phi(x)$, $r''(x) = ag_\sigma(x)$, $r'''(x) = \frac{-ax}{\sigma^2} g_\sigma(x)$. It follows that $r'(x)$ is a *step* edge. The effect of scale on the *concave slope* is the same as on the *step* edge.

We consider now the *roof*; the case of the *valley* is similar. Without loss of generality, we define the *roof* by $t(x) = g_\sigma(x)$. Its first, second and third derivatives are $t'(x) = \frac{-x}{\sigma^2} g_\sigma(x)$, $t''(x) = \frac{1}{\sigma^2}(\frac{x^2}{\sigma^2} - 1) g_\sigma(x)$, $t'''(x) = \frac{-1}{\sigma^4} x(\frac{x^2}{\sigma^2} - 3) g_\sigma(x)$. For all σ (Table 2) $t'(x)$ has a zero-crossing at $x = 0$; $t''(x)$ has a negative minimum which is equal to $\frac{-1}{\sqrt{2\pi}\sigma^3}$ at $x = 0$ and has two zero-crossings (resp. two positive maxima of value $\frac{2e^{\frac{-3}{2}}}{\sqrt{2\pi}\sigma^3}$) at $x = \pm\sigma$ where we have two *steps* (resp. at $x = \pm\sigma\sqrt{3}$), which move away from each other as the scale increases. In $t''(x)$ the absolute value of the minimum is higher than that

x	$-\infty$		$-\sigma\sqrt{3}$		$-\sigma$		0		σ		$\sigma\sqrt{3}$		$+\infty$
$t'(x)$		+		+	*max*	+	0	-	*min*	-		-	
$t''(x)$		+	*max*	+	0	-	*min*	-	0	+	*max*	+	
$t'''(x)$		+	0	-		-	0	+		+	0	-	

Table 2: Effect of σ on a *roof* edge.

of the maximum.

Finally, we study the effect of scale on the *staircase*. An ideal *staircase* is defined by $e_i(x) = c_1 u(x+l) + c_2 u(x-l)$, where c_1 and c_2 represent the contrast at $x = \mp l$ respectively. Let us assume that $c_1 > c_2 > 0$ and $l > 0$ (the case $c_2 \geq c_1 > 0$ is similar). The convolution of $e_i(x)$ with the first and second derivatives of g_σ are $e'(x) = c_1 g_\sigma(x+l) + c_2 g_\sigma(x-l)$, $e''(x) = \frac{-1}{\sigma^2}[c_1(x+l)g_\sigma(x+l) + c_2(x-l)g_\sigma(x-l)]$.

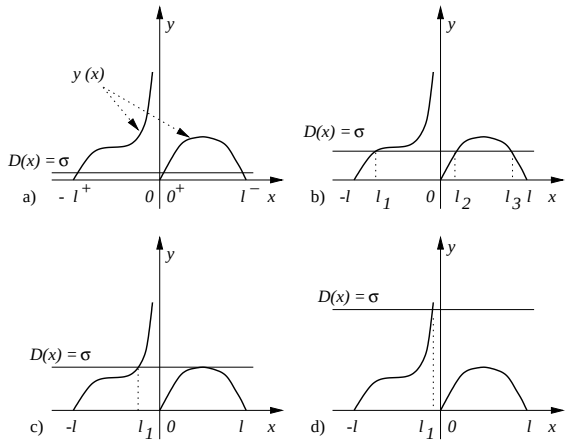

Figure 6: Effect of σ on the sign of the second derivative of the *staircase* in the interval $(-l, l)$.

For all σ we have $e'(x) > 0\ \forall x$, $e''(0) = \frac{-1}{\sigma^2}(c_1 - c_2) l g_\sigma(l) < 0$, $e''(x) > 0\ \forall x \leq -l$, and $e''(x) < 0\ \forall x \geq l$. Let us study the effect of σ on the sign of $e''(x)$. In the case of $x \in (0, l)$, $e''(x) \geq 0$ if $\sigma^2 \leq \frac{2xl}{ln\frac{c_1(x+l)}{c_2(-x+l)}}$, and $e''(x) < 0$ elsewhere. In the case of $x \in (-l, 0)$, $e''(x) \geq 0$ if $\sigma^2 \geq \frac{2xl}{ln\frac{c_1(x+l)}{c_2(-x+l)}}$, and $e''(x) < 0$ elsewhere. Thus, let us consider the function $y(x) = \sqrt{\frac{2xl}{ln\frac{c_1(x+l)}{c_2(-x+l)}}}$, the straight line $D(x) = \sigma$ (Figure 6) and the three following situations. The first, if σ tends towards zero, such that $D(x) \cap y(x) = \{y(-l^+), y(0^+), y(l^-)\}$ (Figure 6.a) where $-l^+, 0^+$, and l^- belong to the vicinity of $-l, 0$, and l respectively, then $e''(x) < 0\ \forall x \in (-l^+, 0)$, and $e''(-l) > 0$. Thus there is a zero-crossing in the vicinity of $x = -l$. $e''(x) > 0\ \forall x \in (0^+, l^-)$, and since we have $e''(0) < 0$ and $e''(l) < 0$, two zero-crossings occur in the vicinity of $x = 0$ and $x = l$ (Table 3.a). The second, if $\sigma > 0$, such that $D(x) < max\{y(x), x \in (0, l)\}$ and $D(x) \cap y(x) = \{y(l_1), y(l_2), y(l_3)\}$ where l_1, l_2 and l_3 belong to $(-l, l)$ (Figure 6.b), then $e''(x) > 0$ if $x \in (-l, l_1) \cup (l_2, l_3)$, and $e''(x) < 0$ if $x \in (l_1, l_2) \cup (l_3, l)$. Consequently, there are three zero-crossings in the vicinity of l_1, l_2 and l_3 (Table 3.b). The third, if $D(x) \geq max\{y(x), x \in (0, l)\}$, let us consider $l_1 \in (-l, 0)$ such that $y(l_1) \in D(x) \cap y(x)$ (Figures 6.c and 6.d). Then $e''(x) > 0\ \forall x \in (-l, l_1)$ and $e''(x) \leq 0\ \forall x \in (l_1, l)$. Thus, we have only one zero-crossing which is located in the vicinity of $x = l_1$ (Table 3.c).

	x	$-\infty$	$-l$			0				l	$+\infty$
	$e'(x)$	+	*max*	+		*min*		+		*max*	+
a)	$e''(x)$	+	+ *zc*	-		- *zc*		+		*zc* -	-

	x	$-\infty$	$-l$		l_1		0		l_2		l_3	l	$+\infty$
	$e'(x)$		+		*max*		+		*min*	+	*max*		+
b)	$e''(x)$		+		*zc*		-		*zc*	+	*zc*	-	

	x	$-\infty$	$-l$			l_1	0				l	$+\infty$
	$e'(x)$			+		*max*			+			
c)	$e''(x)$		+			*zc*	-				-	

Table 3: Effect of σ on a *staircase* edge. a) When $\sigma \to 0$ the *staircase* is located close to $x = 0$. b) When $\sigma > 0$, such as $D(x) < max\{y(x), x \in (0, l)\}$ and $D(x) \cap y(x) = \{y(l_1), y(l_2), y(l_3)\}$; then, if $x \in (0, l)$, min and max of $e'(x)$, as well as the two zc of $e''(x)$, move closer together; if $x \in (-l, 0)$, max of $e'(x)$ and zc of $e''(x)$ move towards $x = 0$. c) When σ increases such that $D(x) \geq max\{y(x), x \in (0, l)\}$ the *staircase* behaves like a *step* in the vicinity of $x = 0$.

5 Classification Algorithm

According to the study of the behavior of edges described in the two previous sections, the rules for the classification of these edges are straightforward (Table 4). To illustrate these rules, let us consider the case of the *step*. The rules of the other types are in [4].

Let us recall that the Laplacian image can contain three classes of characteristic points. Thus in the vicinity $V(P)$ of a pixel P, there are eight possibilities. In the case where P is a *step*, the characteristic point *zero-crossing*$_L$ must belong to $V(P)$ (Table 4). Consequently, the number of combinations is reduced to four ($\{$*zero-crossing*$_L$, $minimum_L$, $maximum_L\}$, $\{$*zero-crossing*$_L$, $minimum_L\}$, $\{$*zero-crossing*$_L$, $maximum_L\}$ and $\{$*zero-crossing*$_L\}$). Let us note that the existence of the characteristic point $maximum_g$ of the gradient image and the *zero-crossing*$_L$ of the Laplacian image in $V(P)$ does not necessarily imply the presence of a *step*. For example, if we have only $\{$*zero-crossing*$_L$, $maximum_L\} \subseteq V(P)$, then the distance between *zero-crossing*$_L$ and P must be lower than that between $maximum_L$ and P. However, P is a *step* edge if it

Edge types	Conditions on the gradient or the first directional derivative	Conditions on the Laplacian
step	$maximum_g > 0$	*zero-crossing*$_L$
concave slope	Inflection point	$maximum_L > 0$
convex slope	Inflection point	$minimum_L < 0$
roof	$zero_g$ or $minimum_g > 0$	$minimum_L < 0$
valley	$zero_g$ or $minimum_g > 0$	$maximum_L > 0$
staircase	$minimum_g > 0$	*zero-crossing*$_L$

Table 4: Rules for the classification of edges. The edge points we are interested are illustrated in Figure 1.

is a $maximum_g$ (Figure 7.a) and one of the following rules holds:

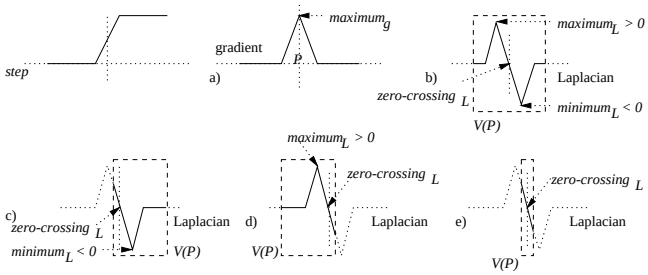

Figure 7: Situations in which a *step* edge is present: a and (b or c or d or e).

- rule 1: $\{$*zero-crossing*$_L$, $minimum_L$, $maximum_L\} \subseteq V(P)$ (Figure 7.b). This means that in the vicinity $V(P)$ of P there are one or more zero-crossings, negative minima, and positive maxima of the Laplacian of the pixel P.

- rule 2: $\{$*zero-crossing*$_L$, $minimum_L\} \subseteq V(P)$ and $\{maximum_L\} \not\subseteq V(P)$ and $Distance(P, \mathcal{C}_{zc}) < Distance(P, \mathcal{C}_{min})$ (Figure 7.c). $\mathcal{C}_{zc}$ (resp. $\mathcal{C}_{min}$, $\mathcal{C}_{max}$) is the set of *zero-crossing*$_L$ (resp. $minimum_L, maximum_L$) of the Laplacian image, which belong to $V(P)$. $Distance(P, \mathcal{C}_{zc})$ (resp. $Distance(P, \mathcal{C}_{min})$, $Distance(P, \mathcal{C}_{max})$) is the distance between P and the closest *zero-crossing*$_L$ (resp. $minimum_L, maximum_L$). This rule means that in $V(P)$ there are only *zero-crossing*$_L$ and $minimum_L$. A *zero-crossing*$_L$ must be the closest to P (cf. Sections 3 and 4).

- rule 3: $\{$*zero-crossing*$_L$, $maximum_L\} \subseteq V(P)$ and $\{minimum_L\} \not\subseteq V(P)$ and $Distance(P, \mathcal{C}_{zc}) < Distance(P, \mathcal{C}_{max})$ (Figure 7.d). This rule means that in $V(P)$ there are only *zero-crossing*$_L$ and $maximum_L$. A *zero-crossing*$_L$ must be the closest to P.

- rule 4: $\{$*zero-crossing*$_L\} \subseteq V(P)$ and $\{maximum_L, minimum_L\} \not\subseteq V(P)$ (Figure 7.e). There are only *zero-crossing*$_L$ in $V(P)$.

It should be noted that these rules reduce the negative effects of missing Laplacian characteristic points in the vicinity $V(P)$ of P.

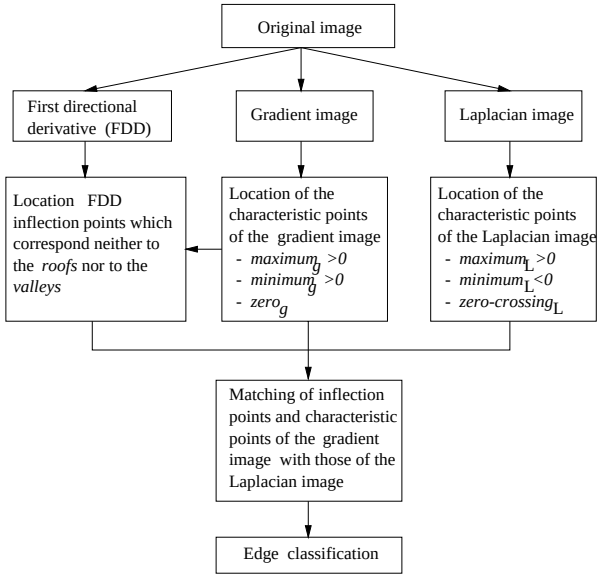

Figure 8: General algorithm for detection and classification of edges.

To summarize, the various stages of our algorithm for detection and classification (or classification alone) are illustrated in Figure 8. The input to this algorithm is the original image and the scale σ of the Gaussian function. As output, it provides edges as well as their type. The algorithm consists of four steps. In the first, using the same scheme as in [11], we calculate the gradient, the first directional derivative, and the Laplacian of the smoothed image. In the second step we locate the characteristic points of the gradient (i.e., $maximum_g, minimum_g, zero_g$) and Laplacian (i.e., $maximum_L, minimum_L,$ *zero-crossing*$_L$) images, as well as the inflection points of the first directional derivative, which are neither in the vicinity of $minimum_g$ nor in that of $zero_g$ [4]. At the $minimum_g$ and $zero_g$ characteristic points, one can have *roof*, *valley* or *staircase* edges. It should be noted that we cleaned up the gradient image by choosing only the characteristic points $maximum_g$ whose modules are higher than a given threshold. In the third step we carry out a matching between the located inflection points or characteristic points of the gradient image, and those of the Laplacian image. The matching algorithm is described

in [4]. Finally, we perform the classification, using twenty four rules.

6 Experimental Results

Our classification has been tested on synthetic images. In the image presented in Figure 9.a we detected *concave slope* and *convex slope* edges with scale $\sigma = 0.95$ (Figure 9.c). At $\sigma = 2$ the locations of *concave slope* and *convex slope* edges did not change; this agree with the theoretical study of the behavior of these edges in the scale space (cf. Section 4). However, a new $step$ edge was created (Figure 9.d), because the scale was large enough to cover both slopes. This demonstrates the possibility that new edges may be created when the scale increases. This new edge can be found using the gradient and Laplacian of Gaussian. This calls into question the results presented in [22, 21], where the authors claim to prove that the Laplacian of Gaussian does not create new edges when the scale increases.

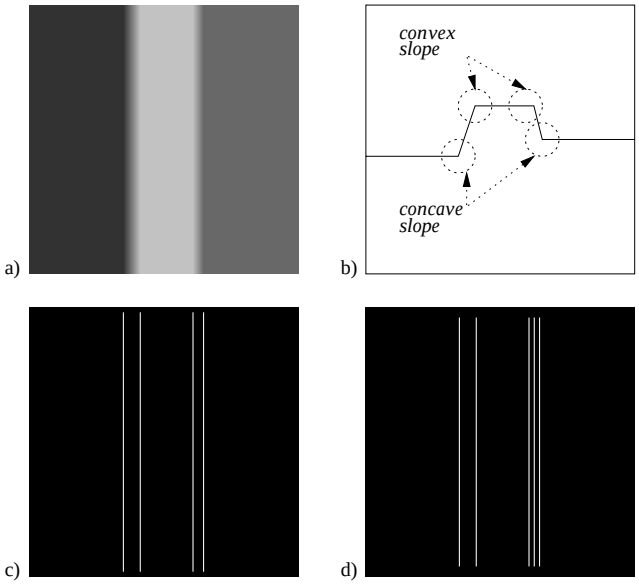

Figure 9: a) Synthetic image. b) Its horizontal profile. c) *Concave* and *convex slope* detected with $\sigma = 0.95$. d) *Concave slope*, *convex slope*, and *step* detected with $\sigma = 2$.

The image illustrated in Figure 10.a contains *step*, *roof*, *valley*, *staircase*, *concave slope* and *convex slope* edges. Those detected with $\sigma = 1$ are shown in Figure 10.c. Figures 10.d, 10.e, and 10.f represent the different classes of edges.

The classification algorithm was run again on the image in Figure 10.a with $\sigma = 2.1$ (Figure 11). Note the disappearance of the *staircase* edge, which is replaced by a *step* edge. The *roof* and *valley* edges move, because they are asymmetrical. There is no displacement of *steps* which are not in the vicinities of the *roof*, *valley*, and *staircase*. The *steps* which

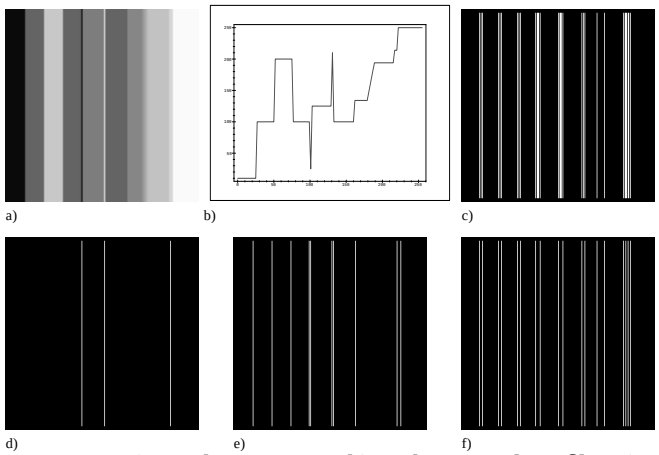

Figure 10: a) Synthetic image. b) Its horizontal profile. c) Edges detected with $\sigma = 1$. d) *Valley* on the left, *roof* in the middle and *staircase* on the right. e) *Step*. f) *Concave slope* and *convex slope*.

are in the vicinities of the *roof* and the *valley* have moved. The two *steps* which are in the vicinity of the *staircase*, are reduced to a single one. Lastly, *concave slope* and *convex slope* edges have moved, except two of them which occupy the third and fourth positions starting from the right edge of Figure 11.d. Indeed, if the scale is too small to overlap these slopes, then they do not undergo displacement. However, note the disappearance of the *convex slope* and the *concave slope* located to the left and right of the *staircase* (Figure 10.b) (cf. Section 4).

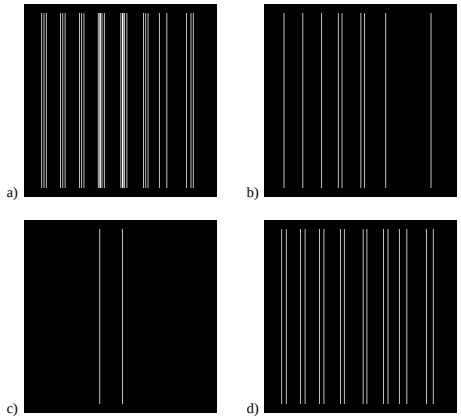

Figure 11: a) All types of edges detected in image 10.a with $\sigma = 2.1$. b) *Step*. c) *Valley* on the left and *roof* on the right. d) *Concave slope* and *convex slope*.

We also tested our algorithm on several real images of 256×256 pixels and 256 grey levels. In Figure 12 we illustrate the classification of edges in the image shown in Figure 12.a. It should be noted that this image is a difficult test for our algorithm. Indeed, it is complex because its edges are close together and the detection of an edge is influenced by

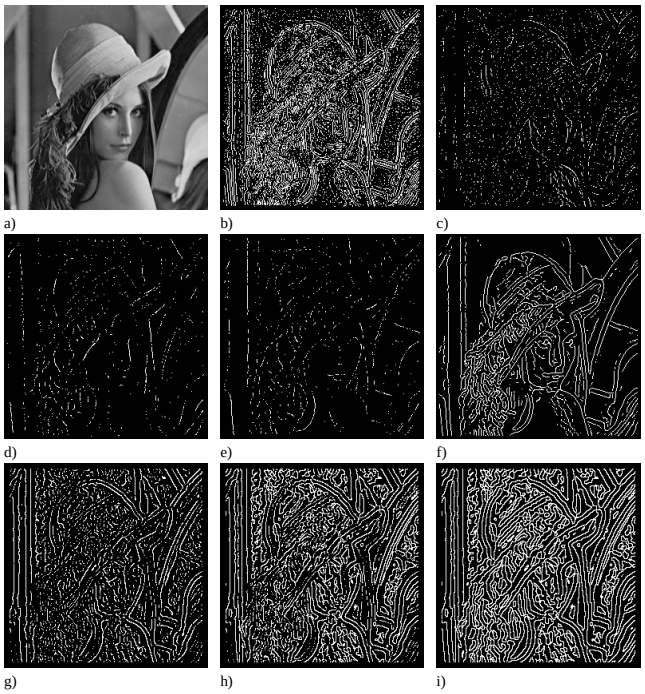

Figure 12: a) Image of Lenna. b) All types of edges, at $\sigma = 1.5$. c) *Staircase*. d) *Roof*. e) *Valley*. f) *Step*. g) *Concave slope* and *convex slope*. h) *Slopes* which are neither *roofs* nor *valleys*. i) All *slopes* without classification.

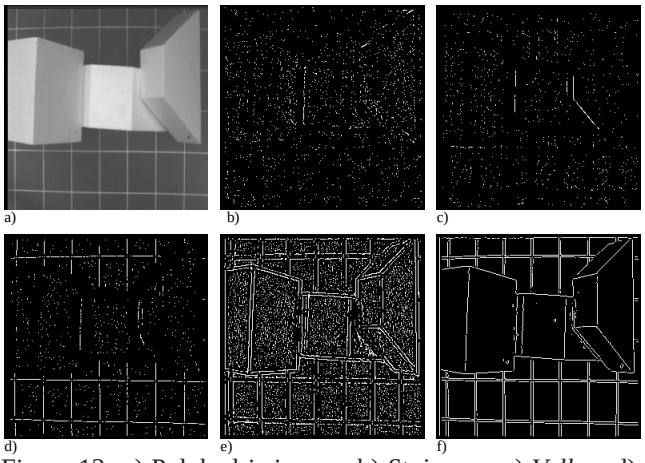

Figure 13: a) Polyhedric image. b) *Staircase*. c) *Valley*. d) *Roof*. e) *Concave slope* and *convex slope*. f) *Step*. The scale used is $\sigma = 1$.

neighboring edges. However, in this image, the significant edges are *steps* (Figure 12.f), *roofs* (Figure 12.d), *valleys* (Figure 12.e) and *slopes* (Figure 12.i). The *steps* and *slopes* are almost continuous, and the other types are incomplete. Finally, we classified the edges of the image illustrated in Figure 13. The edges we detected with a scale $\sigma = 1$ agree with the image intensity profiles.

Note that sometimes there are significant omissions of edges (Figures 11, 12, and 13). This is due to many factors; let us cite three. First, only $maximum_g$ where the value is above a given threshold are considered. Second, only inflection points of the first directional derivative which do not correspond to $zero_g$ and $minimum_g$ are considered. This explains the omission of *concave slope* and *convex slope* edges in Figure 12.h. The third factor is the failure to match characteristic points.

7 Conclusion

We presented some related work on the detection and classification of edges. In order to detect and classify *step, concave slope, convex slope, roof, valley* and *staircase* edges, we studied their behavior with respect to differentiation operators and scale, and derived classification rules accordingly. The reasoning is based on the characteristic points of the first directional derivative, the gradient, and the Laplacian of the image. We considered the case of *step* to illustrate these rules. In order to evaluate our classification, we used synthetic and real grey-level images. Most often, the classification obtained corresponded to the intensity profile of the image. In further work, we will take into account other types of edges such as *junctions*.

References

[1] José R. Beltran, Javier Garcia-Lucia, and Jesus Navarro. Edge Detection and Classification Using Mallat's Wavelet. Proceedings, ICIP-94 Vol.1. Pages 293-297, November 1994.

[2] J.F. Canny. A Computational Approach to Edge Detection. IEEE *Transactions on Pattern Analysis and Machine Intelligence* (PAMI), 8(6):679–698, Nov 1986.

[3] Ezio Catanzariti. Maximum-Likelihood Classification of Image Edges Using Spatial and Spatial-Frequency Features. Proceedings. 11th, IAPR International Conference on Pattern Recognition. Vol.1. Pages 725-729, 1992.

[4] Hanna Chidiac. *Études des contours dans des images à niveaux de gris : origines, détection et classification*. Mémoire, Université de Sherbrooke, Département de mathématiques et d'informatique, Canada, 1998.

[5] R. Deriche. Using Canny's Criteria to Derive a Recursive Implemented Optimal Edge Detector. *The International Journal of Computer Vision*, 1(2):167–187, 1987.

[6] G. Giraudon. Edge Detection from Local Negative Maximum of Second Derivative. *Proceedings of International Conference on Computer Vision and Pattern Recognition* (CVPR), pages 643–645, San-Francisco Ca. (USA), 1985.

[7] R.M. Haralik. Ridge and Valley on Digital Images. *Computer Vision, Graphics and Image Processing*, 22:28–38, 1983.

[8] R.M. Haralik. Second Directional Derivative Zero-Crossing Detector Using the Cubic Facet Model. *Proceedings of 4th Scandinavian Conference on Image Analysis*, pages 17–30, Trondheim, 1985.

[9] Michael D. Heath, Sudeep Sarkar, Thomas Sanocki, and Kevin W. Bowyer. A Robust Visual Method for Assessing the Relative Performance of Edge-Detection Algorithms. IEEE *Transactions on Pattern Analysis and Machine Intelligence* (PAMI), 19(12):1338–1359, december 1997.

[10] E.C. Hildreth. The Detection of Intensity Changes by Computer and Biological Vision Systems. *Computer Vision, Graphics and Image Processing*, 22:1–27, 1983.

[11] Ramesh Jain, Rangachar Kasturi, and Brian G. Schunck. *Machine Vision*. Co-published by the MIT Press and Mc Graw-Hill, Inc, 1995.

[12] K.N.V.L.N. Koundinya and Bhabatosh Chanda. Detecting Lines in Gray Level Images Using Search Techniques. *Signal Processing*, 37(2):287–299, May 1994.

[13] D. Marr and E.C. Hildreth. Theory of Edge Detection. *Proceedings of the Royal Society of London B207*, pages 187–217, 1980.

[14] C. Morrone and R. Owens. Feature Detection from Local Energy. *Pattern Recognition Letters*, 6:303–313, December 1987.

[15] T. Poggio and V. Torre. A Regularized Solution to Edge Detection. Artificial Intelligence lab. Memo, No. 833, Massachusetts Institut of Technology, 1985.

[16] J. Ponce and M. Brady. Toward a Surface Primal Sketch. Three dimensional vision, T. Kanade, Ed. New York: Academic Press, 1985.

[17] M. Robey, G. West, and S. Venkatesh. An Investigation into the Use of Physical Modeling for the Prediction of Various Feature Types Visible from Different Viewpoints. *Computer Vision and Image Understanding*, 61(3):417–429, May 1995.

[18] Jun Shen. On Multi-Edge Detection. *CVGIP: Graphical Models and Image Processing*, 58(2):101–114, march 1996.

[19] A.N. Tikhonov and V.Y. Arsenin. *Solution to Ill-Posed Problems*. Winston and Sons, Washington D.C, 1977.

[20] Svetha Venkatesh and Robyn Owens. On the Classification of Image Feature. *Pattern Recognition Letters*, 11:339–349, May 1990.

[21] L. Wu and Z. Xie. Scaling Theorems for Zero-Crossings. IEEE *Transactions on Pattern Analysis and Machine Intelligence* (PAMI), 12(1):46–54, Jan 1990.

[22] A.P. Yuille and T.A. Poggio. Scaling Theorems for Zero-Crossings. IEEE *Transactions on Pattern Analysis and Machine Intelligence* (PAMI), 8(1):15–25, Jun 1986.

[23] Wei Zhang and Fredrik Bergholm. Multi-Scale Blur Estimation and Edge Type Classification for Scene Analysis. *The International Journal of Computer Vision*, 24(3):219–250, 1997.

[24] D. Ziou. Line Detection Using an Optimal IIR Filter. *Pattern Recognition*, 24(6):465–478, 1991.

[25] D. Ziou and S. Tabbone. Edge Detection Techniques - An Overview. *International Journal of Pattern Recognition and Image Analysis*, 8(4):537–559, 1998.